AIAA JOURNAL
Vol. 50, No. 7, July 2012

Technical Notes

Benchmarking a Coupled Immersed-Boundary-Finite-Element Solver for Large-Scale Flow-Induced Deformation

Rajneesh Bhardwaj* and Rajat Mittal†
Johns Hopkins University, Baltimore, Maryland 21218

DOI: 10.2514/1.J051621

Nomenclature

C_D	=	dimensionless mean drag coefficient, $2F_D^*/(\rho_f U_{\text{mean}}^2 D)$
F_D^*	=	drag force per unit spanwise length on the cylinder and plate, N m^{-1}
D	=	diameter of the cylinder, m
E	=	dimensionless Young's modulus, $E^*/(\rho_f U_{\text{mean}}^2)$
f	=	dimensionless oscillation frequency of the plate, $f^* D/U_{\text{mean}}$
Re	=	Reynolds number, $\rho_f U_{\text{mean}} D/\mu$
U_{mean}	=	mean velocity at the left boundary of the channel, m s^{-1}
V	=	dimensionless dilatational wave speed inside the structure, $\sqrt{E/(\rho_s/\rho_f)}$
Y_{tip}	=	maximum Y displacement of the tip, (Y_{tip}^*/D)
μ	=	dynamic viscosity, N m^{-2} s
ρ_f	=	density of the fluid, kg m^{-3}
ρ_s/ρ_f	=	solid-fluid density ratio

Superscripts

$*$	=	dimensional quantity

I. Introduction

LARGE flow-induced deformation of soft structures with complex material and structural properties as well as complex geometries has numerous engineering applications such as in microaerial vehicles, transport of fluids in elastic structures, energy-harvesting devices, biomedical engineering, and bioinspired systems. The modeling of the flow-induced deformation (FID) for these problems generally involves complex three-dimensional moving solid boundaries and large FID of the structure. The flow in many of the preceding applications is highly unsteady, and the modeling of the structure also involves geometric and material nonlinearities. The coupling of the governing equations of the flow and the structure can lead to complex phenomena such as modal entrainment [1], lock-on, surface morphing, bifurcation, chaotic vibrations, resonance, and stress concentration. Although modeling of the flow and the structure are challenging in their own right, the coupled fluid-structure interaction raises the challenge to an even higher level.

Previous efforts in FID modeling by Dunne and Rannacher [2], Tezduyar et al. [3]and Sahin and Mohseni [4] have mostly employed arbitrary Lagrangian–Eulerian (ALE) methods in which the simulation is performed on a body-conformal mesh, which is modified via a suitable remeshing algorithm at every time step. However, cases involving large deformations and/or topological changes of the boundary pose a severe challenge for the remeshing algorithm. Oftentimes, the remeshing algorithm increases the computational time, and numerical dissipation is needed to provide robustness in the presence of the deformed grid; this can hide the effects of under-resolution of the grid and degrade the solution accuracy. An alternate approach is to employ an immersed boundary (IB) method for the flow simulation. In this method, the governing equations are solved on a fixed Cartesian grid for the flow domain, and the movement of the immersed structure in the fluid is described in a Lagrangian framework. The first IB method was developed by Peskin [5] to simulate cardiovascular dynamics. This method and its variants (see, for example, Zhao et al. [6]) have since been used for a variety of flow problems in engineering and biomechanics [7]. IB-based flow solvers enable the solution of flows with complex moving structure boundaries on stationary Cartesian meshes, and these methods can easily be incorporated in to existing flow solvers [8]. We note that, although FID is a type of fluid-structure interaction (FSI), it is distinguishable from problems that involve flow-induced motion of otherwise rigid structures (such as in Vanella et al. [9] and Eldredge and Pisani [10]) because these latter problems do not require modeling of internal structural stresses. Modeling of these internal structural stresses can introduce additional spatial and temporal resolution requirements that are absent in problems involving FSI of rigid structures.

A second issue in this arena is the limited availability of data sets that can be used to verify the accuracy and fidelity of FID solvers, especially those involving large-scale structural deformation. In this note, we describe a method that couples a sharp-interface IB-method-based flow solver with a finite-element-based structural dynamics solver to construct a robust and versatile solver for FID problems with large-scale deformation. We validate the FID solver against published numerical results and discuss the influence of material properties and geometric nonlinearity on the coupled dynamics of the system. We also extend the benchmark by simulating additional cases with different parameters and material properties.

II. Fluid-Induced Deformation Modeling

The flow solver is a ghost-cell-based sharp-interface immersed boundary method described by Mittal et al. [8]. In this solver, the unsteady, incompressible Navier–Stokes equations are discretized in space using a cell-centered, collocated (nonstaggered) arrangement of primitive variables, i.e., velocity and pressure, and a second-order, central-difference scheme is used for all spatial derivatives. The unsteady Navier–Stokes equation is marched in time using a fractional-step scheme that involves two steps: solving an advection-diffusion equation followed by a pressure Poisson equation. During the first step, both the convective and viscous terms are treated implicitly using the Crank–Nicolson scheme to improve the stability. In second step, the pressure Poisson equation is solved with the constraint that the final velocity be divergence free. The flow solver has been validated for problems such as flow past a circular cylinder, sphere, airfoil, suddenly accelerated normal plate, and suddenly accelerated circular cylinder [8] and is used to simulate a variety of flows [11].

Received 18 September 2011; revision received 2 December 2011; accepted for publication 20 December 2011.

*Department of Mechanical Engineering.
†Department of Mechanical Engineering; mittal@jhu.edu (Corresponding Author).

An open-source, three-dimensional, finite-element solver, Tahoe developed at Sandia National Laboratories, Livermore, CA[‡], is employed for the structural domain. This solver allows a variety of constitutive models and can handle large deformations of multilayered, anisotropic, and heterogeneous structures. The flow computations are performed on an Eulerian grid, whereas the immersed structural surfaces are tracked in a Lagrangian framework. A partitioned (segregated) approach is used to couple the flow and the structure solvers, and an implicit (two-way) coupling between the flow and the structure solvers ensures that the FID solver is stable even for low structure-fluid density ratios [11]. In implicit coupling, outer iterations are performed at each time step until convergence of the coupled system is achieved. In each outer iteration, both the flow and the structure dynamics are solved while updating the boundary conditions at the fluid-structure interface. The coupled system is deemed to have converged when the residual (measured by the L_2 norm of the displacement of the fluid-structure interface) over successive outer iterations reduces below a defined threshold value. The typical threshold value employed is about 4 orders of magnitude lower than the initial residual. The implicit coupling reduces to explicit coupling if only one outer iteration is used.

To enhance the stability to the solver in the face of dynamical nonlinearities, underrelaxation of the displacement and the velocity of the fluid-structure interface is employed. In this scheme, the displacement and the velocity are updated by linearly weighted values of current and previous outer-iteration values by an under-relaxation parameter α [12]:

$$\sum_N \phi_i^{k,\text{new}} = \alpha\phi_i^k + (1-\alpha)\phi_i^{k-1} \tag{1}$$

where ϕ is the displacement or velocity, k is the counter of the outer iteration, N is the number of nodes on the fluid-structure interface, and α is the under-relaxation parameter ($0 < \alpha \leq 1$). Typical values of α used in the simulations range from 0.2 to 0.4, and the final results are found to be independent of the under-relaxation. Although there is significant variation from case to case, 10–20 outer iterations are needed to achieve convergence in the simulations reported in this study.

III. Results and Discussion

A. Comparison with Benchmark

The FID solver is validated quantitatively as well as qualitatively with the benchmark problem proposed by Turek and Hron [13] (TH). The problem consists of a two-dimensional laminar channel flow past a thin elastic plate attached to the lee side of a circular cylinder (Fig. 1). The circular cylinder is rigid and stationary, whereas the elastic plate is deformable. The fluid is considered to be incompressible and Newtonian, whereas the structure is assumed to be elastic and compressible. TH used an implicit, monolithic, ALE method finite-element method (FEM) with a fully coupled multigrid solver [14] for their simulations of both the flow and the structural dynamics.

A parabolic inflow velocity profile is prescribed at the left boundary of the channel with a mean velocity equal to U_{mean}, and an outflow boundary condition is applied on the right boundary (Fig. 1). The constitutive law for the structure is chosen as Saint Venant-Kirchhoff material [15] in which the elasticity of the structure is characterized by Poisson's ratio (ν_s) and Young's modulus (E^*). We also assume a condition of plane strain in the structure and allow full geometric nonlinearity [15] in the structural model.

In addition to the Poisson's ratio and density ratio ρ_s/ρ_f, the two other nondimensional parameters for the problem are the Reynolds number and the dimensionless Young's modulus, which are defined as $Re = \rho_f U_{\text{mean}} D/\mu$ and $E = E^*/(\rho_f U_{\text{mean}}^2)$, respectively, where μ is dynamic viscosity of the fluid, and ρ_f is the fluid density. A comparison of the flowfield, the pressure field, and the plate dynamics with the benchmark is conducted for the following parameters: $\text{D} = 0.1\,\text{m}$, $U_{\text{mean}} = 1\,\text{m}\cdot\text{s}^{-1}$, $\rho_f = 10^3\,\text{kg}\cdot\text{m}^{-3}$,

[‡]Data available online at http://sourceforge.net/projects/tahoe/ [retrieved 11 May 2012].

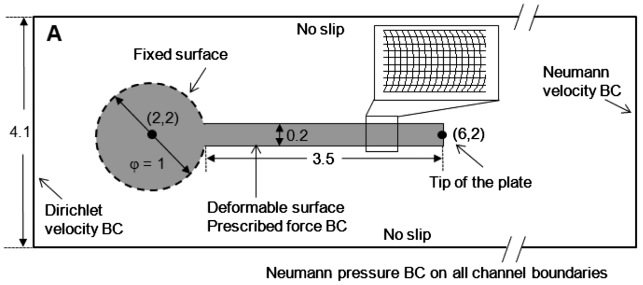

Fig. 1 Schematic and boundary conditions (BC) of the benchmark problem. All numbers shown are dimensionless with respect to the cylinder diameter. The inset shows the finite-element mesh for the plate.

$\rho_s/\rho_f = 10$, $Re = 100$, $E = 1.4 \times 10^3$, and $\nu_s = 0.4$. The domain size in the current simulation is $0 \leq x \leq 11D$ and $0 \leq y \leq 4.1D$, and a 257×129, nonuniform Cartesian grid with $\Delta x_{\min} = 0.023D$ and $\Delta y_{\min} = 0.018D$ is used, wherein high resolution is provided to the region where the plate is expected to move. For the structural solver, the plate is discretized with a total of 1611 quadrilateral finite-elements with $\Delta x_{\min} = 0.02D$ and $\Delta y_{\min} = 0.02D$. The FEM grid in the plate is shown in the Fig. 1 inset. The time step for the flow as well as the structural solver is set to $\Delta t_f = 0.01D/U_{\text{mean}}$, which corresponds to about 50 time steps/period of the plate oscillation. The flow and the structural grid as well as the time step used here were chosen after successive refinement until the computed results became effectively independent of the grid.

Figure 2a shows the computed vorticity field and the deformation of the plate at different time instances. The flow induces a wavelike deformation in the plate, and the plate attains self-sustained periodic oscillation with a constant amplitude after a short time. The time evolution of the Y and X displacements of the plate's tip is shown in Fig. 2b. We note that the plate initially exhibits small deformations and reaches a periodic self-sustained oscillation after a dimensionless time of around 60. The time period and the maximum displacement of the plate are estimated to be about $5.16D/U_{\text{mean}}$ and $0.92D$, respectively.

Figure 3a compares the computed stationary-state results with the published results of TH for the evolution of the displacement of the plate. The values of the oscillation frequency and the maximum Y displacement obtained from our simulation along with the input parameters are given in Table 1 (Case 1a). The dimensionless oscillation frequency ($f = f^* D/U_{\text{mean}}$) is found to be 0.19, which is virtually identical to the value of TH. The differences between the calculated and the published results for the maximum values of Y and X displacement are estimated to be around 11 and 20%, respectively. It should be noted that the larger relative difference in the X displacement is due to the smaller overall magnitude of this quantity. Figure 3b presents a qualitative comparison of the pressure contours and the streamlines at the time when the plate's displacement is at its maximum. The agreement between the present results and those of TH for the shape and magnitude of pressure contours and directions of streamlines is very good.

We also compare the results of a case where $\rho_s/\rho_f = 1$ and $Re = 200$ (Case 1b in Table 1) with the results of TH. In Table 1, the calculated values of the maximum Y displacement and the oscillation frequency for this case are 0.41 and 0.28, respectively. These values are around 14 and 8% larger than the corresponding values in TH, respectively. We note that the system with $\rho_s/\rho_f = 1$ oscillates at a higher frequency than the baseline case ($\rho_s/\rho_f = 10$), and as discussed later in this note, this is consistent with the physics of wave propagation in an elastic plate.

Included in Table 1 are the computed values of the mean drag coefficient. We note that the current computed values for the baseline case as well as Case 1b are 14 and 4% lower, respectively, than the corresponding value of TH. This difference is in line with the fact that the current simulations predict a lower tip amplitude; this reduces the unsteady component of fluctuating shear stresses as shown by Mittal and Balachandar [16] and leads to a lower drag.

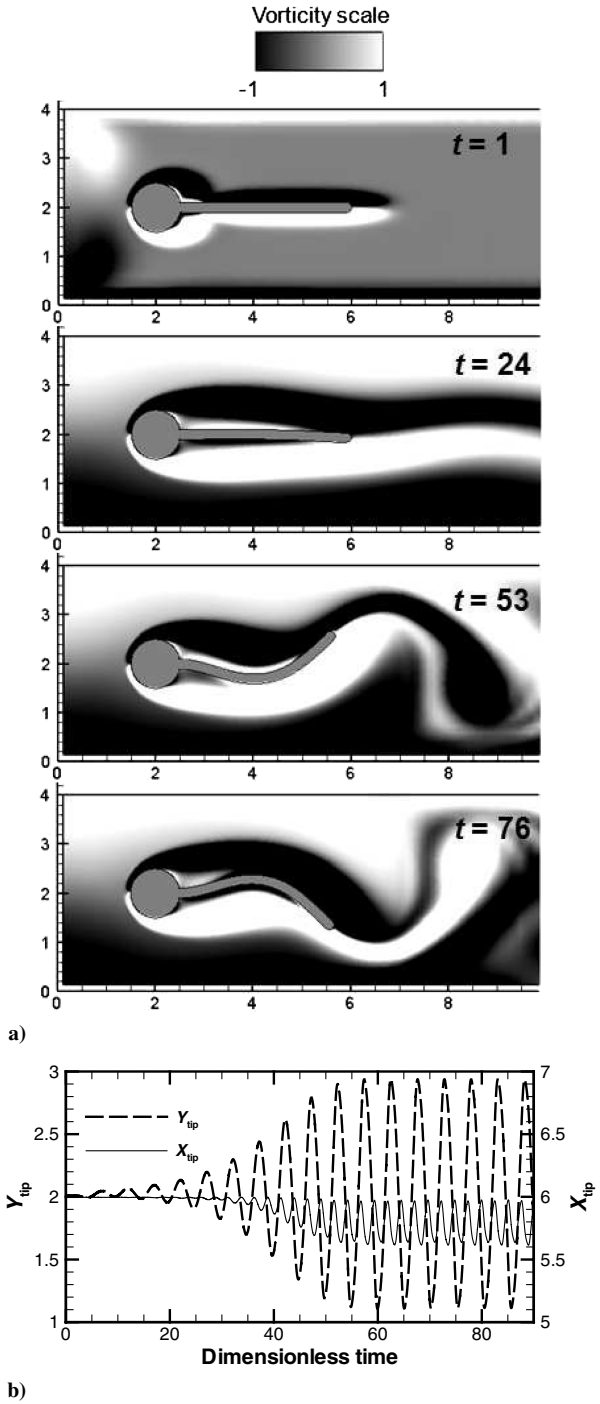

Fig. 2 a) The vorticity field and deformation of the elastic plate shown at different times for the baseline case. b) Temporal variation of *X* and *Y* displacements of the tip of the plate.

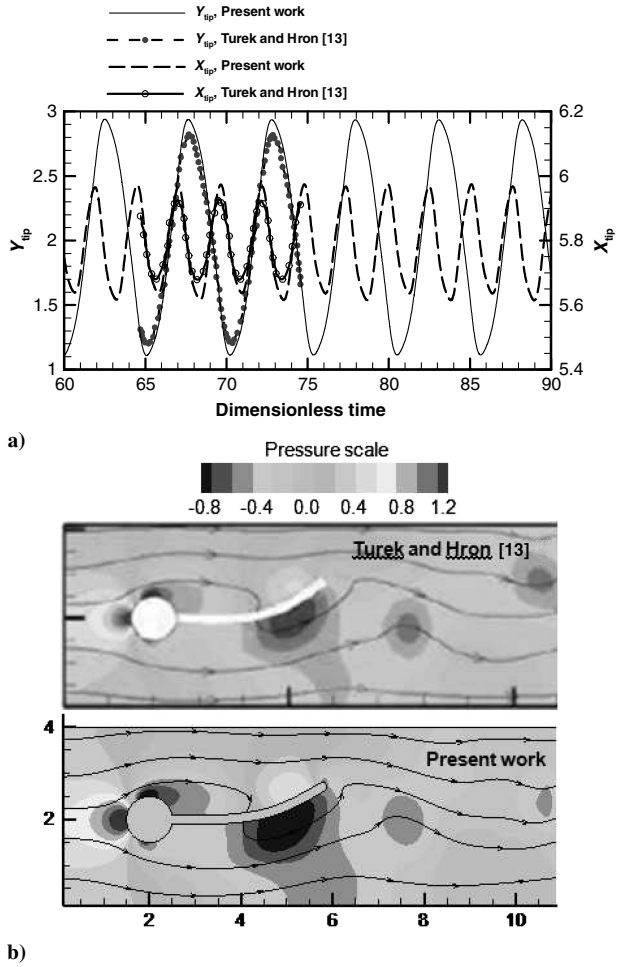

Fig. 3 a) Comparison between the present work and published results of Turek and Hron [13] for the stationary-state time-variation of *X* and *Y* displacement of the tip of the plate. b) Qualitative comparison between the present work and published results of Turek and Hron [13] for pressure contours and streamlines at the time when the *Y* displacement of the tip of the plate is maximum.

The source of the 8–20% mismatch in the vibration amplitude between the current simulations and those of TH is not readily apparent; it could be due to resolution or modeling deficiencies in either the current work or that of TH. In this regard, we note that we have ensured that our results are reasonably grid independent; we have also separately validated the flow solver [8] and the structural solver against canonical problems. However, final assessment of the accuracy of the current FID results will likely require computation of these cases by other methods/simulation codes, and this is the motivation for the rest of the study presented here. The objective of the following sections is twofold: first to understand the effect of key parameters, material properties, and the modeling assumptions on the dynamics of this

Table 1 Different simulation cases considered along with corresponding values for cases simulated by Turek and Hron [13]

Case	ρ_s/ρ_f	Re	Geometric model	E	Y_{tip}	f	C_D
Turek and Hron [13]	10	100	Nonlinear	1.4×10^3	0.83	0.19	4.13
Turek and Hron [13]	1	200	Nonlinear	1.4×10^3	0.36	0.26	2.30
Case 1a (baseline)	10	100	Nonlinear	1.4×10^3	0.92	0.19	3.56
Case 1b	1	200	Nonlinear	1.4×10^3	0.41	0.28	2.20
Case 1c	10	300	Nonlinear	1.4×10^3	1.06	0.21	3.87
Case 2	10	100	Nonlinear	2.8×10^3	0.76	0.24	3.39
Case 3	10	100	Nonlinear	5.6×10^3	0.02	0.29	2.41
Case 4	100	100	Nonlinear	1.4×10^3	0.08	0.08	2.41
Case 5	10	100	Linear	1.4×10^3	1.37	0.19	4.73

configuration and second to provide additional data for this case that can be used by other groups for benchmarking studies in the future.

B. Effect of Reynolds Number

The Reynolds number is a key parameter in this flow, and to quantify the influence of this parameter, we increase this parameter by a factor of 3, keeping all other parameters the same as in the baseline case The calculated values of the maximum Y displacement and the oscillation frequency for this case (Case 1c in Table 1) are 1.06 and 0.21, respectively, which are around 15 and 10% larger, respectively, than the corresponding baseline values. We note that the plate reaches its maximum deformation at a dimensionless time of around 30 for this case, whereas this time is around 60 for the baseline case ($Re = 100$).

C. Effect of Material Properties and Geometric Nonlinearity

We have performed four additional simulations to explore the effect of material properties on the dynamics; in the first two simulations (Cases 2 and 3 in Table 1), the value of the dimensionless Young's modulus E is varied ($E = 2.8 \times 10^3$ and 5.6×10^3) while keeping all other parameters the same as in the baseline configuration described in the preceding sections. In the third simulation (Case 4 in Table 1), the density ratio ρ_s/ρ_f is increased by 1 order of magnitude, keeping all other parameters the same as the baseline case. In the final simulation (Case 5 in Table 1), we examine the effect of geometric nonlinearity on the structural dynamics by recomputing the baseline case with an assumption of a geometrically linear deformation. We note that geometric linearity (or infinitesimal deformation theory) neglects second-order or higher terms in the finite strain tensor [15].

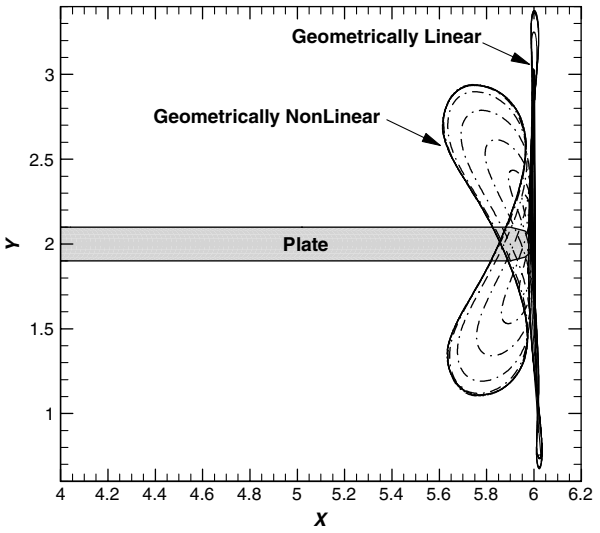

a)

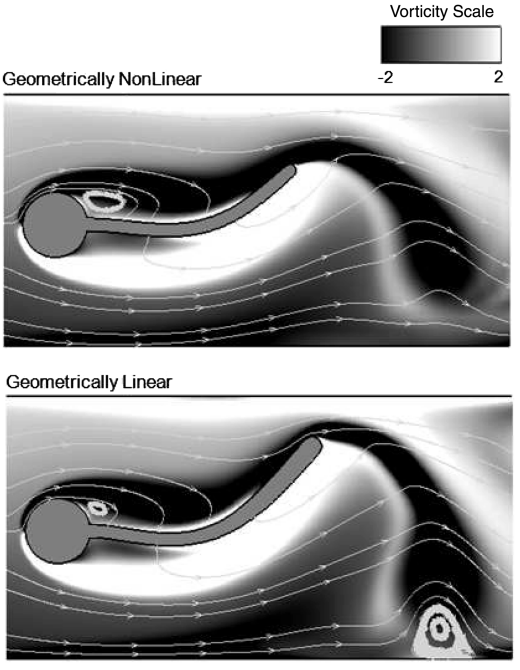

b)

Fig. 4 Influence of geometric nonlinearity: a) trajectories of the plate tip are compared between two cases with and without considering geometric nonlinearity and b) vortex shedding at the instance of maximum tip displacement for the two cases.

Table 1 shows the salient features of all the calculations along with the results of TH. The values of the Y displacement of the tip and the oscillation frequency of the plate for these four cases are shown in Table 1. It is found that the oscillation frequency obtained in simulations (f) varies linearly with the dilatational wave speed (V) inside the structure. The dimensionless expression for V is given by $V = \sqrt{E/(\rho_s/\rho_f)}$, where E is the dimensionless Young's modulus ($E = E^*/(\rho_f U^2_{\text{mean}})$). The best-fit line between f and V for the values in Table 1 is given by $f = 0.011V + 0.052$, with an R^2 value of 0.98.

Figure 4a shows the comparison between the trajectories of the plate tip computed for the baseline and the geometrically linear modeling case. It is noted that the geometrically linear model overestimates the deformation along the x axis. This is because in a geometrically linear formulation, rotational strain is converted into normal strain; consequently, the rotational strain is eliminated at the expense of enhanced lengthening of the plate during its vibration. A qualitative comparison between the flowfields and the plate configuration at the instance of maximum deformation for the two cases is shown in Fig. 4b, and it is noted that the vortex shedding for the geometrically linear case is enhanced because of the larger amplitude of the plate vibration. The figure also shows that for the geometrically linear case, the downstream half of the plate becomes thicker, and this spurious effect is also due to incorrect representation of the rotation in the linear model. Thus, while the frequency of the flapping, even for these cases with large deformation, seems to be well predicted by the linear theory, the details of the deformation of the plate and the motion of its tip are not correctly predicted by the geometrically linear model.

IV. Conclusions

We demonstrate a versatile and robust FID solver, which couples a sharp-interface IB method for the flow simulation with a finite-element-based structural dynamics solver. The proposed high-fidelity FID approach is designed to model relatively complex configurations that involve large-scale FID and an implicit, partitioned (or segregated) approach is implemented to ensure the stability of the solver at low structure-fluid density ratios. A comparison of our results with the corresponding results of TH for the FID of a thin elastic plate attached to a rigid cylinder indicates that the current approach is able to model such configuration with reasonable fidelity. We also assess the influence of the Reynolds number, material properties, and geometric nonlinearity on the plate's deformation. This study provides additional data for benchmarking of FID solvers and also shows clearly the limitations of using geometrically linear deformation models for such cases.

Acknowledgments

This research was supported by the National Science Foundation through TeraGrid resources provided by the National Institute of Computational Science under grant no. TG-CTS100002. R. Mittal would like to acknowledge support from National Science Foundation grant no. CBET-0943425. We thank Thao D. Nguyen and Jung Hee Seo for helpful discussions.

References

[1] Xue, Q., Mittal, R., and Zheng, X., "A Computational Study of the Effect of Vocal-Fold Asymmetry on Phonation," *Journal of the Acoustical Society of America*, Vol. 128, No. 2, 2010, pp. 818.

[2] Dunne, T., and Rannacher, R., "Adaptive Finite Element Approximation of Fluid-Structure Interaction Based on an Eulerian Variational Formulation," *Lecture Notes in Computational Science and Engineering*, edited by H.-J. Bungartz, and M. Schaefer, Springer–Verlag, Berlin/New York/Heidelberg, 2006.

[3] Tezduyar, T. E., Sathe, S., Stein, K., and Aureli, L., "Modeling of Fluid-Structure Interactions with the Space-Time Techniques," *Lecture Notes in Computational Science and Engineering*, edited by H.-J. Bungartz, and M. Schaefer, Springer–Verlag, Berlin/New York/Heidelberg, 2006.

[4] Sahin, M., and Mohseni, K., "An Arbitrary Lagrangian–Eulerian Formulation for the Numerical Simulation of Flow Patterns Generated by the Hydromedusa *Aequorea Victoria*," *Journal of Computational Physics*, Vol. 228, 2009, p. 4588.

[5] Peskin, C. S., "Numerical Analysis of Blood Flow in the Heart," *Journal of Computational Physics*, Vol. 25, 1977, pp. 220–252.

[6] Zhao, H., Freund, J. B., and Moser, R. D., "A Fixed-Mesh Method for Incompressible Flow-Structure Systems with Finite Solid Deformations," *Journal of Computational Physics*, Vol. 227, 2008, pp. 3114–3140.

[7] Mittal, R., and Iaccarino, G., "Immersed Boundary Methods," *Annual Review of Fluid Mechanics*, Vol. 37, 2005, pp. 239–261.

[8] Mittal, R., Dong, H., Bozkurttas, M., Najjar, F. M., Vargas, A., and von Loebbecke, A., "A Versatile Sharp Interface Immersed Boundary Method for Incompressible Flows with Complex Boundaries," *Journal of Computational Physics*, Vol. 227, No. 10, 2008, pp. 4825–4852.

[9] Vanella, M., Fitzgerald, T., Preidikman, S., Balaras, E., and Balachandran, B., "Influence of Flexibility on the Aerodynamic Performance of a Hovering Wing," *Journal of Experimental Biology*, Vol. 212, 2009, pp. 95–105.

[10] Eldredge, J. D., and Pisani, D., "Passive Locomotion of a Simple Articulated Fish-like System in the Wake of an Obstacle," *Journal of Fluid Mechanics*, Vol. 607, 2008, pp. 279–288.

[11] Zheng, X., Xue, Q., Mittal, R., and Beilamowicz, S., "A Coupled Sharp-Interface Immersed Boundary-Finite-Element Method for Flow-Structure Interaction with Application to Human Phonation," *Journal of Biomechanical Engineering*, Vol. 132, 2010, pp. 1–12.

[12] Schafer, M., Heck, M., and Yigit, S., "An Implicit Partitioned Method for the Numerical Simulation of Fluid-Structure Interaction," *Lecture Notes in Computational Science and Engineering*, edited by H.-J. Bungartz, and M. Schaefer, Springer–Verlag, Berlin/New York/Heidelberg, 2006.

[13] Turek, S., and Hron, J., "Proposal for Numerical Benchmarking of Fluid-Structure Interaction Between an Elastic Object and a Laminar Incompressible Flow," *Lecture Notes in Computational Science and Engineering*, edited by H.-J. Bungartz, and M. Schaefer, Springer–Verlag, Berlin/New York/Heidelberg, 2006.

[14] Hron, J., and Turek, S., "A Monolithic FEM/Multigrid Solver for an ALE Formulation of Fluid-Structure Interaction with Applications in Biomechanics," *Lecture Notes in Computational Science and Engineering*, edited by H.-J. Bungartz, and M. Schaefer, Springer–Verlag, Berlin/New York/Heidelberg, 2006.

[15] Fung, Y. C., *Foundations of Solid Mechanics*, 2nd ed., Springer–Verlag, Berlin/New York/Heidelberg, 1993.

[16] Mittal, R., and Balachandar, S., "Effect of Three-Dimensionality on the Lift and Drag of Nominally Two-Dimensional Cylinders," *Physics of Fluids*, Vol. 7, No. 8, 1995, pp. 1841–1865.

Z. Wang
Associate Editor